

The Engineer's Guide To EMI In DC-DC Converters (Part 13): Predicting The Common-Mode Conducted Noise Spectrum

by Timothy Hegarty, Texas Instruments, Phoenix, Ariz.

The high-frequency and high-edge-rate voltages and currents caused by power device switching within a dc-dc converter can generate spectrally rich conducted and radiated electromagnetic interference (EMI) within the converter itself, as well as in nearby susceptible circuits. This can result in the generation of conducted emissions (CE) with amplitudes exceeding the allowed limits in the frequency band defined by applicable electromagnetic compatibility (EMC) standards. Therefore a committed mitigation effort is typically necessary to comply with these standards.

The work of EMI mitigation is made more challenging by the continuing trend of higher-density converters with smaller packaging, which places active and passive components in close proximity. Such proximity results in an enhancement of parasitic couplings, both capacitive and inductive, creating a complex high-frequency electromagnetic environment.

Part 1 of this article series^[1-12] reviewed the applicable EMI standards and measurement approaches for conducted and radiated interference from dc-dc converters. Part 2 then studied the noise propagation and separation of differential-mode (DM) and common-mode (CM) currents to understand the requisite attenuation from the EMI filter, while part 7 reviewed an isolated flyback converter and the CM displacement current in the transformer's interwinding capacitance.

More recently, part 12 reviewed the DM noise spectrum and streamlined models to predict it, at least from a low-frequency standpoint as it pertains to DM filter design. The analysis considered the converter and passive EMI filter stage as well as the measurement equipment, specifically the line impedance stabilization network (LISN) and the EMI test receiver. Part 13 now takes a similar approach for the CM conducted noise spectrum, again referring to the behaviors of the converter, the passive EMI filter and the LISN.

There are of course some differences in this new analysis. For example, to predict the DM noise spectrum, we modeled the converter input current and estimated its harmonic content by Fourier analysis. Here the converter CM noise source is modeled as a voltage source.

Common-Mode Noise Excitation And Propagation

As discussed in part 12, DM noise is essentially caused by normal current flow within the power-delivery path of the operating converter circuit. The DM current propagation path is therefore made up of input capacitors, input cables and traces, and connectors such as threaded terminals and ring lugs.

CM noise current, on the other hand, flows through the earth or chassis ground (GND) connection^[2,7] and is dictated by the amplitude as well as the slew rates (dv/dt) of the switching voltage waveform(s). The CM noise propagation path comprises mainly stray capacitances to GND from the supply cables or traces and—more importantly—the parasitic capacitance between the switching device and its heatsink structure to GND.

Fig. 1 shows the DM and CM current paths in a typical EMI measurement setup using two LISNs (one for each dc power lead) for EMI measurement. Denoted explicitly are the capacitive parasitics from the converter and load to the reference GND plane to complete the CM current path.

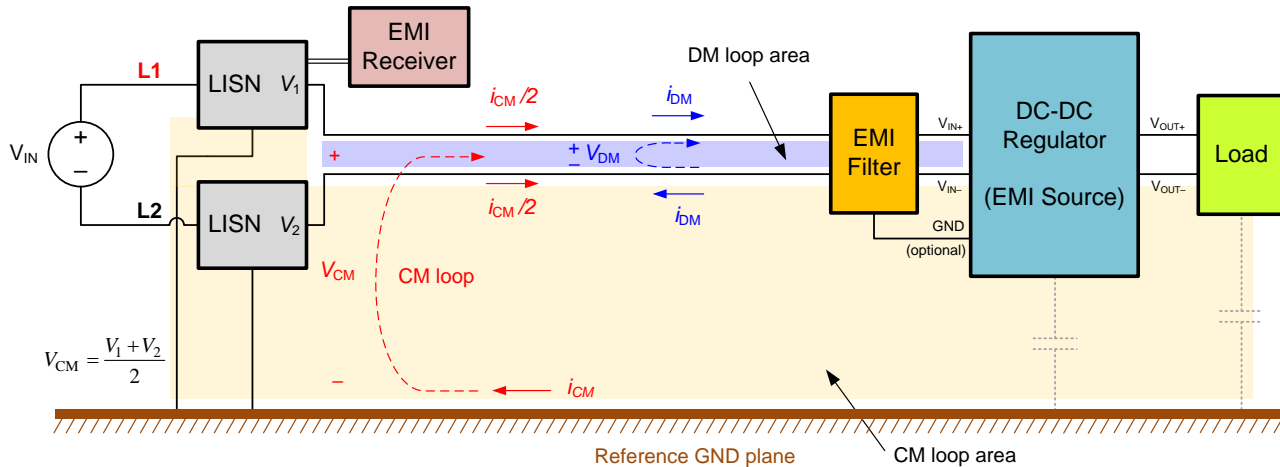


Fig. 1. EMI measurement setup. The large effective loop area of the CM current represents a major source of radiated EMI and contrasts with the relatively small DM current-loop area.

As depicted in Fig. 1, the CM voltage is the average voltage of the two supply lines with respect to a reference GND plane, and the CM current is the sum of the currents flowing in parallel and in the same direction along the supply lines and returning via the GND plane. The shaded loop areas in Fig. 1 indicate the regions of the circuit that can couple with external fields. You can see that the CM conduction loop represents a much larger area than the DM loop.

In general, CM-conducted noise significantly impacts the magnetic near-field radiated EMI signature^[13] given the large CM loop area of the power-supply cables. Moreover, CM emissions especially dominate at high frequencies, as the applicable noise source impedance is generally of a capacitive nature.

Common-Mode Filtering

Fig. 2a presents a conventional π -stage EMI filter for a dc-dc regulator with integrated DM and CM filter stages. Fig. 2b shows the CM equivalent filter circuit decomposition.^[2] This decoupling assumes that the EMI filter has a perfectly symmetric circuit structure and that the board layout is also symmetric.^[14,15]

The uncoupled DM inductors (designated L_{DM1} and L_{DM2}) are placed on both the positive and negative lines to provide common-mode balance, and appear in parallel from a CM standpoint. The total effective inductance contributed by the CM ferrite choke (L_{CM}) and the symmetric DM inductors breaks against the Y-capacitance (C_{Y1} and C_{Y2}) connected to GND and forms a second-order CM filter with an attenuation characteristic of -40 dB per decade. The Y-capacitors offer low shunt impedance for the CM currents to circulate locally in a tight loop area, close to their generating source: the power switches.

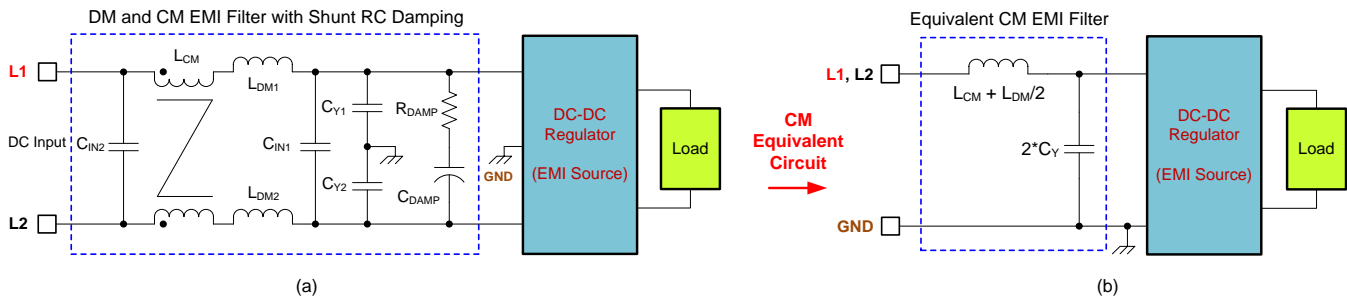


Fig. 2. Typical EMI filter with integrated DM and CM stages using discrete passive components and a balanced circuit structure (a) and decoupled equivalent circuit for CM noise currents (b).

As a caveat, however, component and structural parameters in a practical application may not be ideally symmetric, making it difficult to decouple the DM and CM filter circuits. DM-to-CM noise transformation and vice versa can occur due to these asymmetries.^[14] For example, if C_{Y1} and C_{Y2} are not exactly the same in Fig. 2, part of the CM noise would transform to DM noise.

Also noteworthy in Fig. 2 is that the Y-capacitors are typically not incorporated in two-wire, low-voltage dc-dc converter systems, owing to the lack of an available chassis GND connection. The CM inductance in such implementations acts by itself to increase the series impedance of the CM current loop, resulting in an attenuation characteristic of -20 dB per decade, at least up to the self-resonant frequency of the CM choke.

Model Of A CM EMI Filter

Fig. 3 shows an EMI measurement setup for a synchronous buck converter based on the CISPR 25:2016 international specification,^[12] which is similar to the GB/T 18655-2018 Chinese standard.

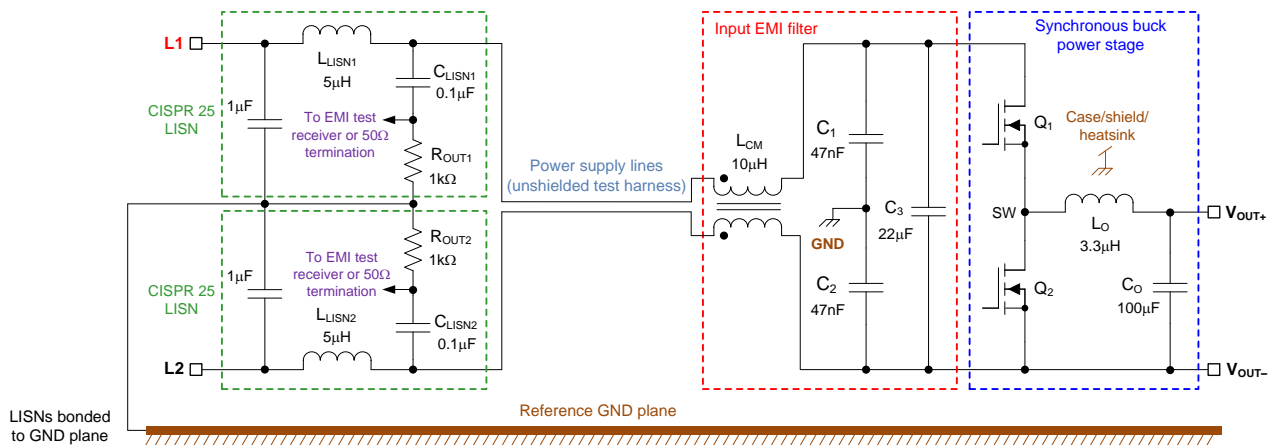


Fig. 3. Schematic diagram of a typical CISPR 25 CE test platform (voltage method) for a synchronous buck regulator, with a single-stage CM filter and LISN connected at each input power lead.

According to the impedance mismatch criteria for EMI filter design, and given the high source impedance and low load impedance of the CM noise circuit, the design uses a Γ -shaped filter (CL topology) for CM noise suppression. Here the Y-capacitors face the dc-dc converter and the dotted terminals of the CM choke attach to each LISN as shown.

The selected components in Fig. 3 set the corner frequency of the single-stage CM filter at approximately 165 kHz. The CM choke provides a rated impedance of 630 Ω at 10 MHz, equivalent to an inductance of 10 μ H. Furthermore, the leakage inductance of the CM choke acts as a DM filter inductance. Fig. 3 omits the filter damping network for circuit simplification.

If we take the component values for L_{CM} , C_{Y1} and C_{Y2} from the EMI filter in Fig. 3 and apply them to the equivalent input EMI filter (together with parasitic and damping network values) we obtain the equivalent CM EMI filter shown in Fig 4a. We can then obtain the current attenuation of the filter as plotted in Fig. 4b. The resonances^[16,17] are based on a CM choke dc resistance (DCR) of 200 m Ω , an equivalent parallel resistance (EPR) of 50 k Ω and an equivalent parallel winding capacitance (EPC) of 10 pF. Also, the Y-capacitor equivalent series resistance (ESR) is 5 m Ω and the equivalent series inductance (ESL) is 0.5 nH.

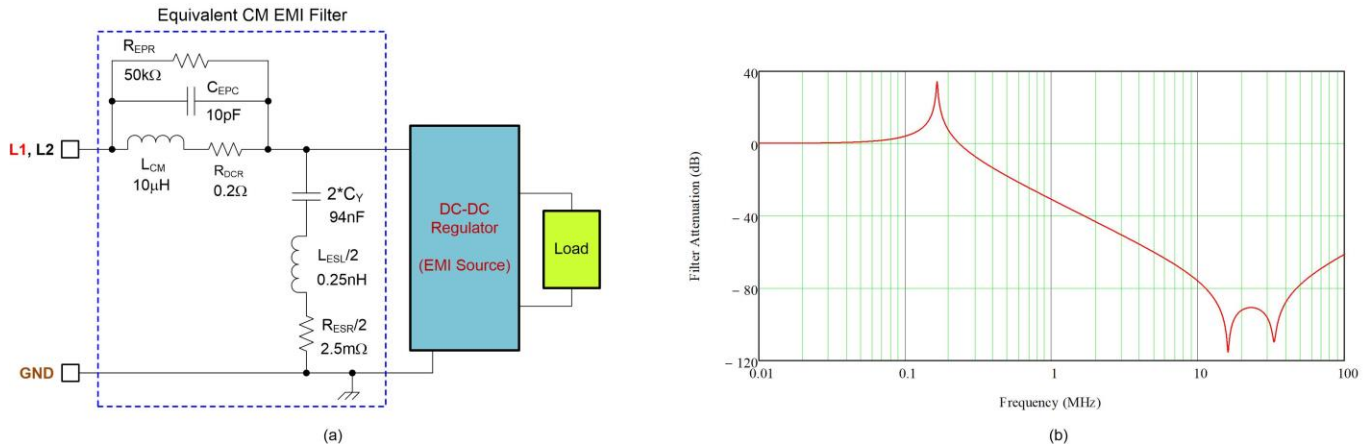


Fig. 4. Equivalent CM input filter schematic for the EMI filter in Fig. 3 (a) and its frequency response (b). This plot of the filter’s current attenuation includes higher-order resonances related to the filter component self-parasitic elements, specifically the DCR, EPR and EPC of the choke and the ESR and ESL of the Y-capacitors.

CM Model Of The LISN

Also included in Fig. 3 on each supply line, L1 and L2, is a LISN measurement circuit with component values as defined in CISPR 25 Annex E. The values are similar for a LISN conforming to CISPR 16, the main difference being a higher LISN inductance of 50 μ H. CISPR 16 and CISPR 25 LISNs are designed to operate up to 30 MHz and 108 MHz, respectively, based on the applicable frequency ranges for conducted emissions.

Fig. 5 shows a CM equivalent circuit of the LISN in the mid-to-high frequency range (150 kHz to 108 MHz applies to CISPR 25 CE). An equivalent voltage source denoted as V_{CM} replaces the converter. The spectral composition of the switch-voltage waveform defines this voltage source, an example being the trapezoidal voltage waveform of a buck converter.

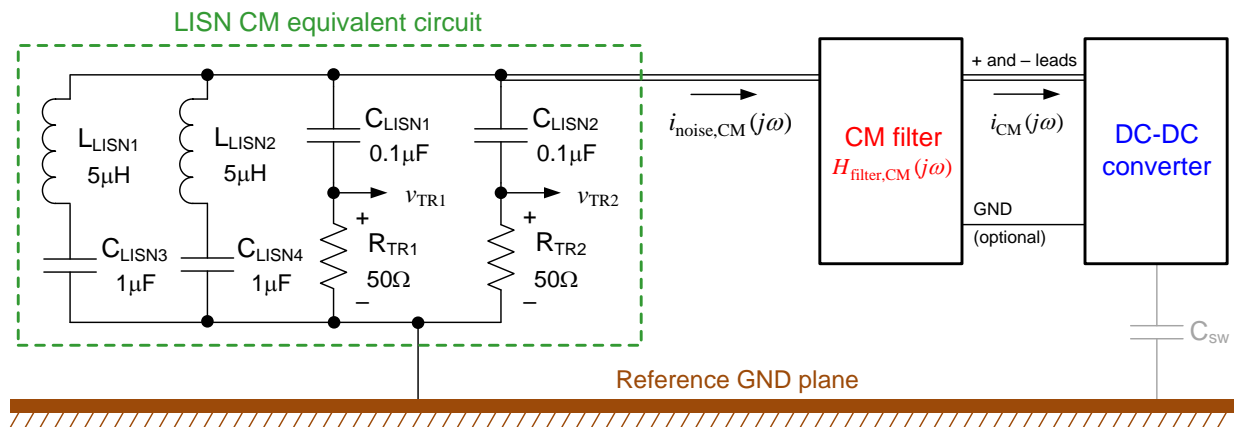


Fig. 5. A simplified high-frequency circuit model, assuming a balanced CM noise path, for determining CM conducted emissions through calculations or numerical simulation. A CM equivalent voltage source designated as V_{CM} (not shown) models the converter’s switching behavior.

The model in Fig. 5 is a good fit for circuit analysis, calculation of attenuation and estimation of impedances if the equivalent noise source is modeled correctly. Equation 1 gives the LISN transfer function from the filtered CM noise current to the LISN disturbance voltage (when connected to and measured by the EMI receiver):

$$G_{\text{LISN}}(s) = \frac{v_{\text{TR1}}(s)}{i_{\text{noise,CM}}(s)/2} = \frac{s^2 L_{\text{LISN1}} C_{\text{LISN3}} + 1}{s^2 L_{\text{LISN}} C_{\text{LISN3}} + s R_{\text{TR}} C_{\text{LISN3}} + [1 + C_{\text{LISN3}}/C_{\text{LISN1}}]} \cdot R_{\text{TR}} \quad (1)$$

Using equation 1, Fig. 6 plots the LISN transfer function over frequency using the component values in Fig. 5. Also included is an equivalent plot for a CISPR 16 LISN that has a 10 times higher LISN inductance. The transfer function is essentially the same as that presented in part 12 for a DM perspective.

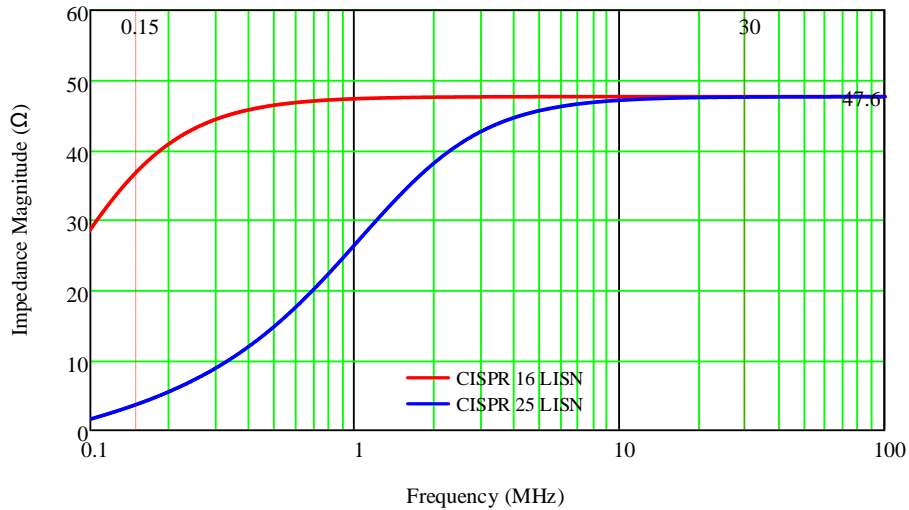


Fig. 6. Plot of LISN transfer function from input noise current to measured output voltage.

While both curves in Fig. 6 converge at high frequencies to 47.6 Ω, corresponding to the parallel combination of the 50-Ω input resistance of the test receiver with the 1-kΩ discharge resistance of the LISN, CISPR 25 specifies a lower LISN inductance of 5 μH, shunting more current from the measurement resistor at low frequencies. The effective impedance of a CISPR 25 LISN is surprisingly low below 1 MHz (5 Ω at 200 kHz), much lower than the nominal 50 Ω presented by the test receiver.

Referring to Fig. 5 and using the frequency-domain transfer functions of the LISN and input filter, equation 2 calculates the measured voltage spectrum $v_{\text{TR}}(j\omega)$ at the LISN output for a given spectrum of CM current $i_{\text{CM}}(j\omega)$:

$$v_{\text{TR}}(j\omega) = i_{\text{noise,CM}}(j\omega) G_{\text{LISN}}(j\omega) = [i_{\text{CM}}(j\omega) H_{\text{filter,CM}}(j\omega)] G_{\text{LISN}}(j\omega) \quad (2)$$

Assuming an ideal decoupling of the converter from the input supply at high frequencies due to the LISN inductance, and a perfect coupling with the test receiver by the LISN 0.1-μF capacitance, the high-frequency equivalent CM circuit of the LISN corresponds to $G_{\text{LISN}}(j\omega) = 47.6 \Omega$. The most simplified CM model of the two-LISN setup comprises the two measurement resistors in parallel, usually approximated as a total of 25 Ω.

When configured in a practical test setup as described in part 2, the LISN presents the total noise comprising DM and CM voltage components. A passive or active DM-CM noise separator circuit is then required to extract the CM noise signature. Treating the DM and CM components separately helps streamline the EMI filter design process—an upcoming installment of this article series will provide further context on this important topic.

CM Noise Model Of The Converter

The proper identification of the noise spectra followed by measurement with a test receiver enables an early determination of filtering requirements and an efficient filter design workflow. As presented in part 12, equation 3 gives a periodic function $S(t)$ by an infinite sum of sinusoidal components based on Fourier analysis:

$$S(t) = c_0 + \sum_{n=1}^{\infty} 2|c_n| \cos(n\omega_s t + \angle c_n) \tag{3}$$

$$c_n = \frac{1}{t_s} \int_{t_0}^{t_0+t_s} S(t) e^{-jn\omega_s t} dt$$

where n is the harmonic order and t_s is the period.

The Fourier series expansion coefficients for $n \geq 1$ are multiplied by a factor of 2 in equation 3 to account for a one-sided spectrum of positive frequencies. As an example, equation 4 provides the harmonic magnitudes for the switch-node voltage of a dc-dc buck converter:

$$c_n(d, n) = V_{in} d \left| \frac{\sin(n\pi d)}{n\pi d} \right| \left| \frac{\sin(n\pi d_r)}{n\pi d_r} \right| \tag{4}$$

where V_{in} is the input voltage and d is the converter duty cycle.

A second term set by finite rise and fall times of the voltage waveform, t_R and t_F , sets the duty factor d_r . Plotted in Fig. 7, the harmonic envelope of the trapezoidal voltage is a double sinc function with corner frequencies of f_1 and f_2 , depending on the pulse width and rise and fall times of the time-domain waveform.^[4] The spectral envelope initially rolls off with frequency at a rate of -20 dB per decade and then transitions to -40 dB per decade after a break frequency f_2 that increases with higher dv/dt .

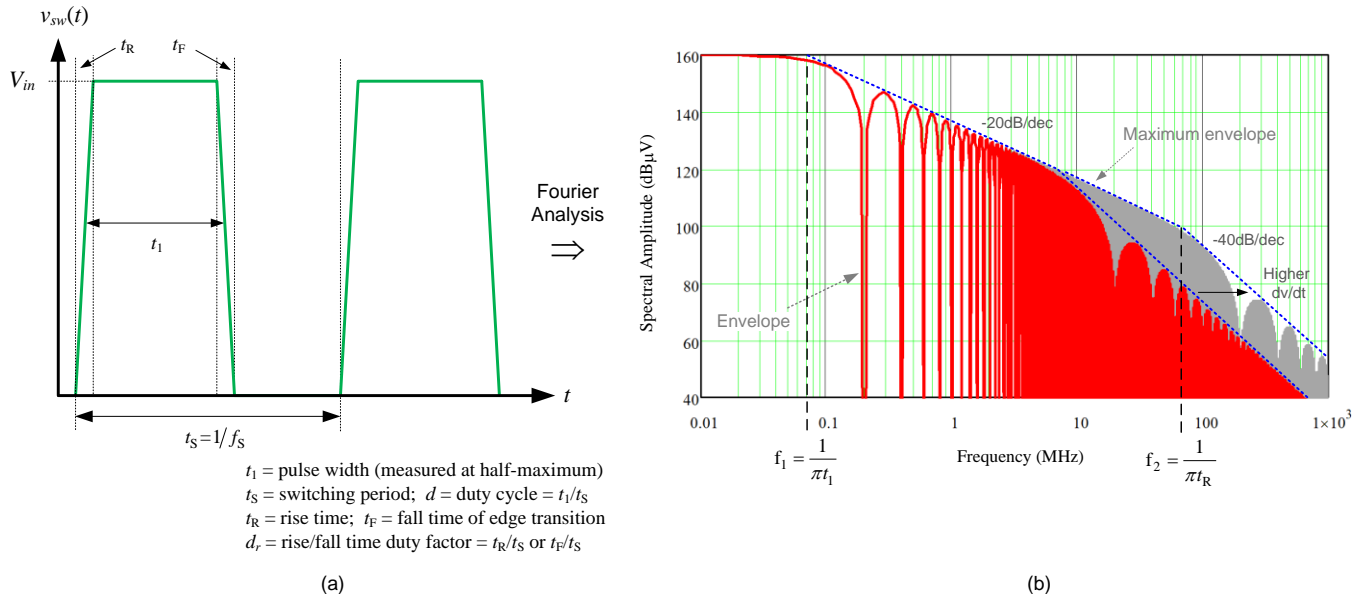


Fig. 7. Buck converter switch-node voltage waveform with $V_{in} = 100$ V, $f_s = 100$ kHz and $D = 50\%$ (a) and its spectral envelope plotted using equation 4 is impacted by the rise and fall times of 10 ns (gray) and 100 ns (red) (b).

A ringing characteristic at the edges of the voltage waveform (from power-loop parasitic inductance) can be represented by including the applicable frequency components from the measured voltage waveform. Due to the high amplitude of $v_{sw}(t)$, the disturbance current in the wider 150-kHz to 108-MHz frequency range applicable to CISPR 25 is easily formed by parasitic parameters and finally causes CM current to flow in the supply lines. The switching frequency, duty cycle, and rise and fall times are effectively constant for a given load current during a particular test—the CM noise then relates to the disturbance current propagation paths.

Simplified CM Noise Model Of The Converter And Measurement Setup

Fig. 8 shows simplified lumped-element CM and DM models^[18] for a dc-dc buck converter and its conducted EMI test setup. While the CM model is the main focus in this article, included in Fig. 8b for additional context is the DM model (see also part 12).

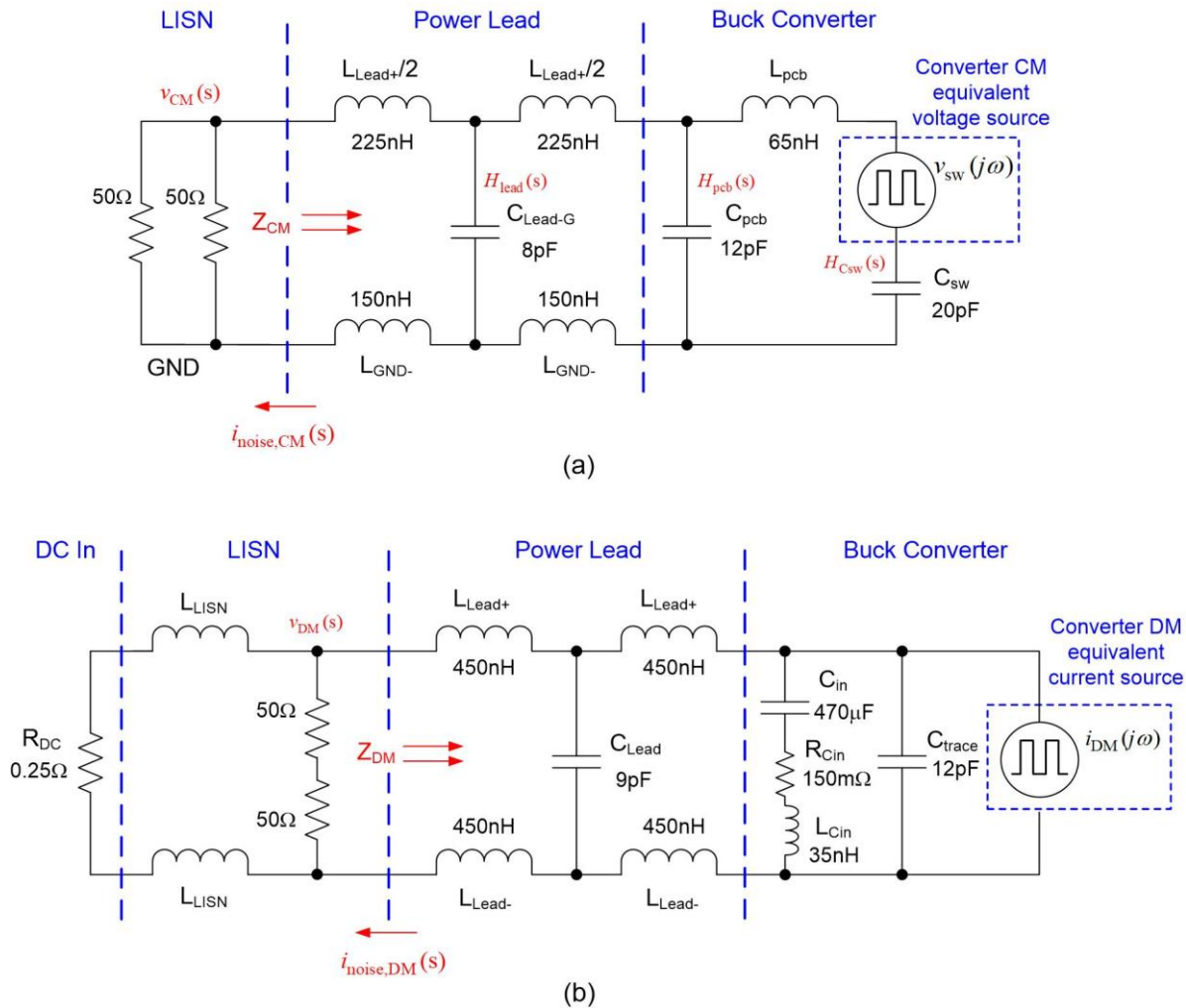


Fig. 8. Simplified CM (a) and DM (b) noise models of the converter measurement setup.

The CM model shows the voltage source v_{sw} of the trapezoidal switching waveform and its parasitic capacitance C_{sw} to GND that includes the effect of a heatsink structure if attached. Two parallel resistors of $50\ \Omega$ represent the LISN noise impedance. C_{pcb} is the effective capacitance from the power traces to the GND plane under the converter. L_{Lead+} designates the power feed-line inductance to the dc-dc converter, and C_{Lead-G} is the

capacitance of the power feed lines to the GND plane. L_{GND} - denotes the parasitic inductance of the GND plane return.

Such power feed line and GND plane parameters are deduced from a series of open- and short-circuited impedance measurements based on transmission line models. The values in Fig. 8 originate from a MIL-STD-461G conducted EMI setup^[19] with a supply feed line length and spacing of 1.2 m and 2 cm, respectively, set at a height of 5 cm above the GND plane.

Referring to the CM noise model in Fig. 8a, equation 5 defines the frequency-domain transfer function as the ratio of the CM disturbance voltage v_{CM} to the noise source voltage v_{sw} as follows:

$$H_{CM}(s) = \frac{v_{CM}(s)}{v_{sw}(s)} \quad (5)$$

Replacing the converter noise source $v_{sw}(s)$ in the CM transfer function with $v_{Csw}(s)$, $v_{lead}(s)$ or $v_{pcb}(s)$ creates the respective transfer functions $H_{Csw}(s)$, $H_{lead}(s)$ and $H_{pcb}(s)$ as referenced in Fig. 8a, where:

- $H_{Csw}(s)$ is the ratio of the parasitic switch capacitance voltage v_{Csw} to the measured CM voltage v_{CM} ;
- $H_{pcb}(s)$ is the ratio of the PCB capacitance voltage v_{Cpcb} to v_{CM} ;
- $H_{lead}(s)$ is the ratio of the power-lead capacitance voltage $v_{Clead-G}$ to v_{CM} .

These transfer functions benchmark the impact a particular branch has on the CM disturbance over a given frequency range. As an example, Fig. 9a presents the calculated CM transfer function magnitudes from 10 kHz to 200 MHz.

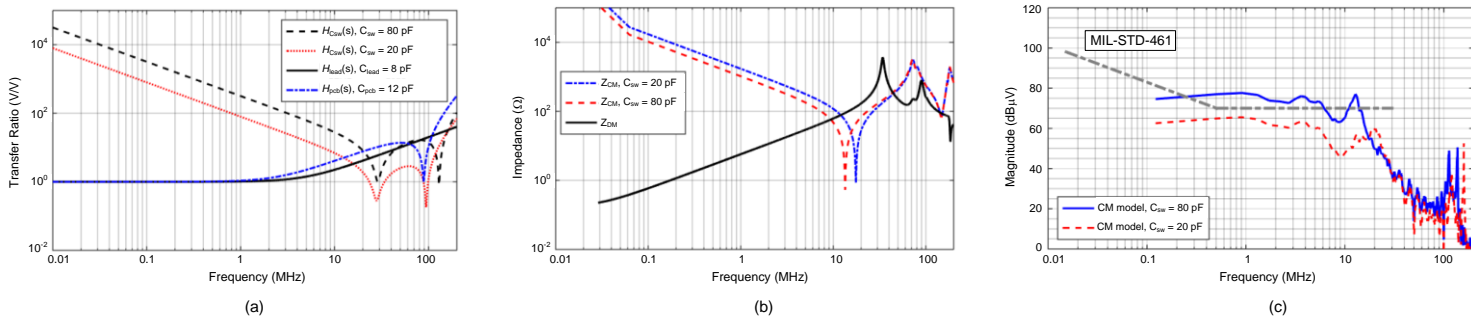


Fig. 9. CM transfer function characteristics (a), DM and CM impedances (b) and CM noise spectral envelope plot (c).

As a general observation with this example, the transfer function $H_{Csw}(s)$ related to the parasitic switch capacitance dominates in the lower frequency band below 20 MHz. The capacitance C_{pcb} becomes more prominent beyond 20 MHz, whereas the power-lead capacitance C_{Lead-G} tends to dominate above 100 MHz.

Fig. 9b plots the calculated DM and CM impedances for two values of C_{sw} . The advantage of higher source impedance related to C_{sw} for CM noise is below 10 MHz. Meanwhile, Fig. 9c shows the CM noise spectral envelope obtained from the model, based on a switch waveform of 100 kHz with 50% duty cycle and rise and fall times of 100 ns.

Summary

A major impediment to the ongoing proliferation of power electronic systems is the spectrally rich emissions produced by high-frequency and high-edge-rate switching behavior. Preventing such emissions (of which CM voltage and current comprise an important subset) from producing EMI requires a detailed understanding.

This article examined the CM conducted noise spectrum using Fourier analysis of the switch-voltage waveform and a simplified lumped-element CM noise model. The parasitic capacitance of the switches to ground generally represents the CM noise source impedance for a buck converter. An upcoming installment of this article series will consider CM filter design, leveraging the concepts outlined here to streamline the filter design procedure.

References

1. ["The Engineer's Guide To EMI In DC-DC Converters \(Part 1\): Standards Requirements And Measurement Techniques,"](#) by Timothy Hegarty, How2Power Today, December 2017 issue.
2. ["The Engineer's Guide To EMI In DC-DC Converters \(Part 2\): Noise Propagation And Filtering,"](#) by Timothy Hegarty, How2Power Today, January 2018 issue.
3. ["The Engineer's Guide To EMI In DC-DC Converters \(Part 3\): Understanding Power Stage Parasitics,"](#) by Timothy Hegarty, How2Power Today, March 2018 issue.
4. ["The Engineer's Guide To EMI in DC-DC Converters \(Part 4\): Radiated Emissions,"](#) by Timothy Hegarty, How2Power Today, April 2018 issue.
5. ["The Engineer's Guide To EMI In DC-DC Converters \(Part 5\): Mitigation Techniques Using Integrated FET Designs,"](#) by Timothy Hegarty, How2Power Today, June 2018 issue.
6. ["The Engineer's Guide To EMI In DC-DC Converters \(Part 6\): Mitigation Techniques Using Discrete FET Designs,"](#) by Timothy Hegarty, How2Power Today, September 2018 issue.
7. ["The Engineer's Guide To EMI In DC-DC Converters \(Part 7\): Common-Mode Noise Of A Flyback,"](#) by Timothy Hegarty, How2Power Today, December 2018 issue.
8. ["The Engineer's Guide To EMI In DC-DC Converters \(Part 8\): Common-Mode Noise Mitigation In Isolated Designs,"](#) by Timothy Hegarty, How2Power Today, February 2019 issue.
9. ["The Engineer's Guide To EMI In DC-DC Converters \(Part 9\): Spread-Spectrum Modulation,"](#) by Timothy Hegarty, How2Power Today, August 2019 issue.
10. ["The Engineer's Guide To EMI In DC-DC Converters \(Part 10\): Input Filter Impact On Stability,"](#) by Timothy Hegarty, How2Power Today, November 2019 issue.
11. ["The Engineer's Guide To EMI In DC-DC Converters \(Part 11\): Input Filter Impact On Dynamic Performance,"](#) by Timothy Hegarty, How2Power Today, January 2020 issue.
12. ["The Engineer's Guide To EMI In DC-DC Converters \(Part 12\): Predicting The Differential-Mode Conducted Noise Spectrum,"](#) by Timothy Hegarty, How2Power Today, April 2020 issue.
13. ["Modeling and analysis of conducted and radiated emissions due to common mode current of a buck converter"](#) by Mohammed Laour et al., *IEEE Transactions on Electromagnetic Compatibility* 59, No. 4 (August 2017): 1260-1267.
14. ["Investigation of the transformation between differential-mode and common-mode noises in an EMI filter due to unbalance"](#) by Shuo Wang and Fred Lee, *IEEE Transactions on Electromagnetic Compatibility* 52, No. 3 (August 2010): 578-587.

15. "[Generalized differential-common-mode decomposition for modeling conducted emissions in asymmetric power electronic systems](#)" Aaron Brovont, *IEEE Transactions on Power Electronics* 33, No. 8 (August 2010): 6461-6466.
16. "[Characterization of common mode chokes at high frequencies with simple measurements](#)" by Carlos Domínguez-Palacios et al., *IEEE Transactions on Power Electronics* 33, No. 5 (May 2018): 3975-3987.
17. "[A high frequency equivalent circuit and parameter extraction procedure for common mode choke in the EMI filter](#)" by Wenhua Tan et al., *IEEE Transactions on Power Electronics* 28, No. 3 (March 2013): pp. 1157-1166.
18. "[Analysis, modelling and measurement of the effects of aluminium and polymer heatsinks on conducted electromagnetic compatibility in DC-DC converters](#)" by Inus Grobler and Michael Gitau, *IET Science, Measurement & Technology* 11, No. 4 (July 2017): 414-422.
19. "[Requirements for the control of electromagnetic interference characteristics of subsystems and equipment](#)," MIL-STD-461G, Dept. of Defense Interface Standard, December 2015.

About The Author



Timothy Hegarty is an applications engineer for the Buck Switching Regulators business unit at Texas Instruments. With over 23 years of power management engineering experience, he has written numerous conference papers, articles, seminars, white papers, application notes and blogs.

Tim's current focus is on enabling technologies for high-frequency, low-EMI, isolated and nonisolated regulators with wide input voltage range, targeting industrial, communications and automotive applications in particular. He is a senior member of the IEEE and a member of the IEEE Power Electronics, Industrial Applications and EMC Societies.

For more information on EMI, see How2Power's [Power Supply EMI Anthology](#). Also see the How2Power's [Design Guide](#), locate the Design Area category and select "EMI and EMC".